



CHORUS

This is the accepted manuscript made available via CHORUS. The article has been published as:

Indications of flow near maximum compression in layered deuterium-tritium implosions at the National Ignition Facility

M. Gatu Johnson *et al.*

Phys. Rev. E **94**, 021202 — Published 15 August 2016

DOI: [10.1103/PhysRevE.94.021202](https://doi.org/10.1103/PhysRevE.94.021202)

Indications of flow near maximum compression in layered DT implosions at the National Ignition Facility

M. Gatu Johnson¹, J.P. Knauer², C.J. Cerjan³, M.J. Eckart³, G.P. Grim³, E.P. Hartouni³, R. Hatarik³, J.D. Kilkenny⁴, D.H. Munro³, D.B. Sayre³, B.K. Spears³, R.M. Bionta³, E.J. Bond³, J.A. Caggiano³, D. Callahan³, D.T. Casey³, T. Döppner³, J.A. Frenje¹, V.Yu. Glebov², O. Hurricane³, A. Kritcher³, S. LePape³, T. Ma³, A. Mackinnon³, N. Meezan³, P. Patel³, R.D. Petrasso¹, J.E. Ralph³, P.T. Springer³, and C.B. Yeamans³

¹Massachusetts Institute of Technology Plasma Science and Fusion Center, Cambridge, MA 02139, USA

²Laboratory for Laser Energetics, University of Rochester, Rochester, NY 14623, USA

³Lawrence Livermore National Laboratory, Livermore, CA 94550, USA

⁴General Atomics, San Diego, CA 92186, USA

An accurate understanding of burn dynamics in implosions of cryogenically layered deuterium and tritium (DT) filled capsules, obtained partly through precision diagnosis of these experiments, is essential for assessing the impediments to achieving ignition at the National Ignition Facility (NIF). We present measurements of neutrons from such implosions. The apparent ion temperatures (T_{ion}) are inferred from the variance of the primary neutron spectrum. Consistently higher DT than DD T_{ions} are observed, and the difference is seen to increase with increasing apparent DT T_{ion} . The line-of-sight r.m.s. variations of both DD and DT T_{ion} are small, ~ 150 eV, indicating an isotropic source. DD neutron yields are consistently high relative to the DT neutron yields given the observed T_{ions} . Spatial and temporal variations of the DT temperature and density, DD-DT differential attenuation in the surrounding DT fuel, and fluid motion variations contribute to DT $T_{\text{ion}} > DD T_{\text{ion}}$, but are in a 1D model insufficient to explain the data. We hypothesize that in a 3D interpretation, these effects combined could explain the results.

At the National Ignition Facility (NIF) [1], cryogenically layered capsules of deuterium and tritium (DT) fuel contained in 2-mm diameter carbon-based shells are imploded through laser irradiation of a surrounding high-Z hohlraum [2-3]. The imploding DT fuel assembles and “stagnates” in a configuration with a cold, high-density shell surrounding a low-density hot-spot. Efficient conversion of shell kinetic energy to hot-spot thermal energy is an essential requirement to achieving ignition at the NIF [4,5]. At peak convergence, this ideally results in a spherically symmetric, cold, dense DT fuel shell with an areal density (ρR) of ~ 1.5 g/cm² surrounding a ~ 5 keV hot-spot with $\rho R \sim 0.3$ g/cm². Although the word “stagnation” is often used for this phase of the implosion, it is inappropriate as the DT and DD neutron spectra indicate significant remaining kinetic energy. Neutron spectrometers [6-15] provide directional measurements of DT and DD neutron spectra from which yield, burn-averaged ion temperatures (T_{ion}) and ρR 's are obtained. Neutron activation detectors (NAD) [16] measure the un-scattered DT yield (Y_{DT}). In this paper, we focus on the ion “temperatures” from a more extensive set of experiments than previously published [2], and conclude that the fuel assembly during burn in layered DT implosions is not well described by detailed 1D physics models and simulations. The leading hypothesis for the observed discrepancy between the data and the 1D description is significant disordered motion and the highly 3D nature of the assembly at burn.

For a homogeneous, stationary DT plasma in thermal equilibrium at ion temperature T_{thermal} , the variance of the DT neutron spectrum (in units of neutron energy) is given by

$$\sigma^2 = \frac{2T_{\text{thermal}} E_n m_n}{(m_n + m_\alpha)}, \quad (1)$$

where E_n is the neutron energy and m_n , m_α are the fusion product masses [17-20]. This has been traditionally used to infer T_{ion} [21,22]. For DD neutrons the denominator is $(m_n + m_{3\text{He}})$, giving a 25% larger relative neutron spectral broadening for the same T_{thermal} because of the higher average thermal velocity of the

reactants. It should be noted that the strong coupling of deuterons and tritons will result in equality of the true ion temperatures. In a recent paper, Murphy [23] articulates that the quantity inferred from the neutron spectrum variance, which we will call apparent T_{ion} , for a homogeneous, non-stationary plasma is the sum of the thermal broadening and a macroscopic broadening from the line-of-sight-projected bulk fluid velocity variance, σ_v^2 ,

$$T_{\text{ion,apparent}} = T_{\text{thermal}} + \frac{(m_d + m_x)}{k_B} \sigma_v^2, \quad (2)$$

where k_B is Boltzmann's constant, and $m_x = m_t$ for DT neutrons, $m_x = m_d$ for DD (see also [24]). If the variance of the bulk velocity dominates over T_{thermal} , then apparent T_{ion} as inferred from the neutron spectrum variance for DD neutrons will be 80% of the apparent T_{ion} inferred from DT neutrons. For the implosions studied here, the apparent T_{ion} is inferred (using the formalism developed in Ref. 20) from the variance of the neutron spectrum produced in a plasma known to be non-homogeneous. In this scenario, one has to consider what impact fuel elements at different T_{thermal} (and possibly different σ_v^2) have on the primary neutron spectrum. Clearly, there is a significant amount of information encoded in the width of the neutron spectral peaks.

The capability to measure DD T_{ion} in a DT implosion is a recent development, first reported in Ref. 25 and on NIF in Ref. 26. The measurement is now made at the NIF with unprecedented precision and accuracy [10]. The simultaneous measurement of DT and DD neutron yield (Y_{DD}) and apparent T_{ion} in DT implosions is achieved with a suite of three nearly orthogonal, fast neutron Time-Of-Flight (nTOF) detectors [9-11]. These detectors [27] are fielded at polar and azimuthal angles, with respect to the hohlraum axis and target positioner, of 116-316, 90-174 and 161-056. Two other neutron spectrometers, the NITOF nTOF detector at 90-315 [12] and the Magnetic Recoil neutron Spectrometer (MRS) at 73-324 [13-15], also provide independent measurements of apparent DT T_{ion} . Unless otherwise stated, the apparent T_{ion} values discussed in this paper are the

weighted averages from all reporting spectrometers for each implosion.

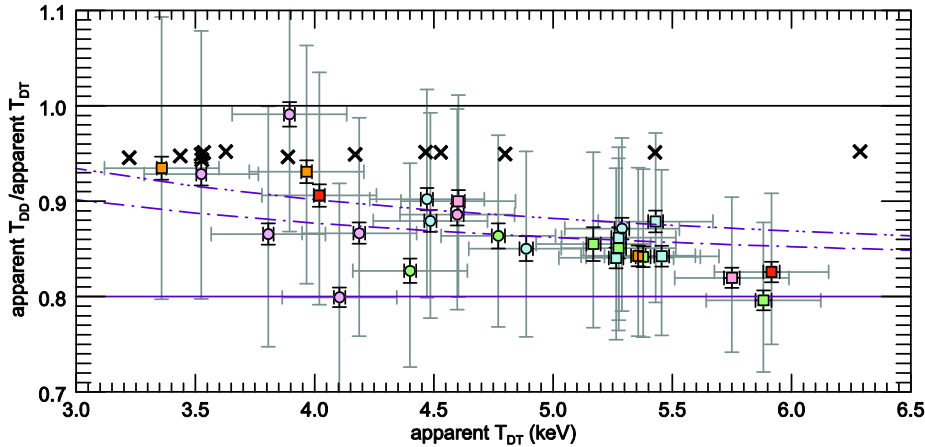


Figure 1: Ratio of apparent DD to DT T_{ion} as a function of apparent DT T_{ion} . The data points come from cryogenically layered NIF DT implosions, with HiFoot-driven 195 μm CH ablator shots in green, 175 μm CH ablator shots in blue and 165 μm CH ablator shots in pink, HDC shots in purple, and shots driven with an adiabat-shaped laser pulse in orange. A square point indicates that the implosion utilized a depleted uranium hohlraum; circular points represent Au hohlraum implosions. Red points indicate shots with a known asymmetry in the laser drive and/or fuel. Gray error bars represent the systematic error, black error bars represent the statistical error. Also shown are simulated ratios from 1D HYDRA simulations (black crosses) and predicted ratios in apparent T_{ion} due to a non-thermal contribution from flows according to ref [23], assuming a thermal $T_{\text{ion}} = 0$ keV (solid purple line), thermal $T_{\text{ion}} = 1.5$ keV (dot-dashed line) and thermal $T_{\text{ion}} = 2$ keV (double-dot dashed line).

In this paper, we examine the neutron data from cryogenically layered DT implosions driven with the so-called HiFoot [2-3] or adiabat-shaped [28] laser pulse. The data set includes implosions with 165, 175 and 195 μm thick CH ablator [29] and high-density carbon (HDC) ablator [30], in gold or depleted uranium (DU) hohlraums [31,32]. The ρR 's for all implosions range from 0.4 to 1.1 g/cm^2 (ρR is determined from the measured neutron down-scatter ratio (DSR) [8,33-34]).

Figure 1 shows the ratio of the measured apparent DD T_{ion} to apparent DT T_{ion} plotted as a function of apparent DT T_{ion} (different-colored points with error bars represent different implosion types, as detailed in the figure caption). A trend in the DD to DT T_{ion} ratio with increasing apparent T_{ion} is observed, which appears independent of ablator material and thickness, hohlraum material, and laser pulse shape. A number of possible mechanisms have been proposed that would give rise to $DT T_{\text{ion}} > DD T_{\text{ion}}$ in these implosions. These include flows [23], species separation [35], and Knudsen tail depletion [36,37]. However, before any such effects are invoked to describe the data, it is important to consider that a difference in measured apparent DT and DD T_{ion} is also expected based on the spatial and temporal burn weighting of the neutron emission because of the different temperature dependence of the DD and DT reactivities [38].

The neutron spectrum measurements discussed here are all integrated over the burn history of the plasma; measured spectra include neutrons from all regions and times in the non-homogeneous plasma hot and dense enough for fusion reactions to occur. The fusion burn lasts <250 ps during which time there are strong spatial gradients; the capsule starts out at $\sim 2\text{mm}$ diameter, is compressed a factor ~ 25 at the fuel ablator radius,

and consists at the time of burn of a dense (many 100's of g/cm^3) cold fuel shell surrounding a central, lower-density (many 10's of g/cm^3) hotspot with temperature that peaks in the center and drops off dramatically towards the hotspot-to-high-density-shell interface. Since the DD and DT reactivities increase steeply with increasing temperature, the neutron-based observations weight towards higher temperature. The relatively higher DD reactivity at lower temperature will result in a burn-averaged apparent DD $T_{\text{ion}} < DT T_{\text{ion}}$. In addition, the cross section for DD neutron elastic scattering in the dense fuel shell is larger than that for DT neutrons. Given a relatively higher cold fuel ρR at times with high T_{ion} than at times with low T_{ion} , this differential attenuation effect integrated over space and time can also contribute to observed apparent DD $T_{\text{ion}} < DT T_{\text{ion}}$.

The impact of profile effects on the T_{ion} ratio is assessed using the HYDRA code [39]. The black crosses in Figure 1 are results from 1D HYDRA simulations for some of the implosions studied here, where the laser drive has been artificially adjusted for perfectly symmetric capsule illumination (i.e., the radiation field has been smeared around the capsule so that it sees a uniform radiation drive, see Ref. 40 for more detail). Running the code in this mode effectively eliminates any velocities during burn in the simulation, and the resulting simulated T_{ion} ratio is expected to be almost entirely due to profile effects. The simulations are done post-shot, and constrained by a requirement to reproduce measured values for, e.g., burn duration (τ_{burn}), implosion velocity (v_{imp}), hot-spot radius (r_0) and DSR [40]. For these implosions, τ_{burn} is measured by the Gamma Reaction History (GRH) detector [41], DSR by the neutron spectrometers, and hotspot size by the neutron imager (NIS) [42].

Hydrodynamically equivalent Convergent Ablator (ConA) implosions are used to determine v_{imp} [43]. Comparing the simulated black crosses with the data in Figure 1, it is clear that 1D profile effects alone do not explain the observations.

Bulk fluid flow will impact the measured neutron spectrum, as discussed in the introduction (Eq. 2) and in Refs. 23, 24, 41, contributing to apparent $DT T_{\text{ion}} < DT T_{\text{ion}}$. The magnitude of this effect is illustrated as a function of apparent $DT T_{\text{ion}}$ in Figure 1, where the solid purple line shows the calculated expected T_{ion} ratio due to non-thermal motion assuming zero T_{thermal} , the dot-dashed line the T_{ion} ratio due to non-thermal motion assuming $T_{\text{thermal}}=1.5$ keV, and the double dot-dashed line the T_{ion} ratio due to non-thermal motion assuming $T_{\text{thermal}}=2$ keV. If we assume the observed temperature difference is due to flow, then the inferred average T_{thermal} for many of the shots is very low (more than half the shots fall below the double dot-dashed 2 keV T_{thermal} line). Correcting for profiles using the T_{ion} ratio from 1D HYDRA simulations (black crosses in Figure 1), T_{thermal} is on average 2.1 keV for implosions with T_{ion} ratio lower than predicted from the simulations. Such low T_{thermal} requires a much higher than previously calculated pressure ($Y_{\text{DT}} \sim P^2 T_{\text{ion}}^2$) [45], and hence hot spot density, to reconcile measured τ_{burn} , r_0 and neutron yields. Higher hot-spot density is inconsistent with X-ray irradiance measurements on these implosions. We conclude that in a 1D model, combined profile/reactivity related effects and flows are insufficient to explain the measured T_{ion} ratios.

It is also interesting to study the relative DT/DD yields from these implosions. In Figure 2, measured $Y_{\text{DT}}/Y_{\text{DD}}$ (colored data points) are contrasted to predictions based on Bosch-Hale reactivities [38] assuming a fuel ratio of 50:50 D:T (solid black line) and 60:40 D:T (dot-dashed black line). Weighted average yields from all reporting detectors (nTOF, MRS and NAD) are used. Note that the data points are plotted versus measured apparent $DT T_{\text{ion}}$, while the theoretical curves assume the x-axis represents T_{thermal} . Due to the high ρR , a significant fraction of neutrons lose energy through scattering on ions in the cold fuel, which has to be considered when measuring the yields. Measured yield is defined as the integral from $E_n=2.2-2.7$ MeV for Y_{DD} and from $E_n=13-15$ MeV for Y_{DT} (points without error bars in Figure 2). Birth yields (framed data points with error bars) are inferred from measured yields using correction factors as a function of DSR determined from MCNPX modeling of a 1D implosion [46,47]. The vertical error bars in Figure 2 represent the statistical uncertainty in the yield ratio measurement. The systematic uncertainty is represented by the dotted gray curves relative to the dashed curve average for the framed data points. Errors in the DSR measurement are also considered when determining these total statistical and systematic errors in the DSR -corrected yield ratio measurement.

In principle, since the DT/DD reactivity ratio is a strong function of temperature, the yield ratio is another thermometer that can be brought to bear to determine hot-spot plasma conditions [48]. This method requires, however, (i) high accuracy in the birth yield ratio measurements, and (ii) a thorough understanding of the isotopic composition of the fuel. Given the present uncertainties in both of these factors, T_{thermal} for these implosions cannot be constrained to a meaningful accuracy using this method. In regards to fuel isotope composition, targets for these implosions are filled with a 50:50 mixture of DT gas. However, due to different freezing temperatures for D and T, it is estimated that the solid ice layer in the cryogenic capsules contains 50%:50% D:T, while the composition of the vapor in the

central cavity before the implosion is 63%:37% D:T. The mass of the vapor is $\sim 0.8 \mu\text{g}$. Estimated total mass of the reacting fuel for these implosions ranges from 4-13 μg , meaning the effective D fraction should be in the range of 50.8%-52.3%, and the corresponding T fraction in the range of 47.7%-49.2%. Taking these best-estimate numbers at face value, the DD yield comes in higher than expected relative to the DT yield for a majority of these implosions. Measured and predicted yields could be reconciled if apparent $DT T_{\text{ion}}$ was inflated due to flows. However, it cannot at present be ruled out that shot-to-shot variations in the fuel isotope composition may be as high as $\pm 10\%$.

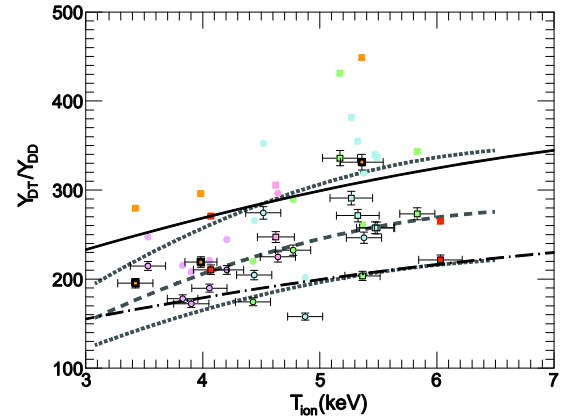


Figure 2: DT-to-DD yield ratios as a function of $DT T_{\text{ion}}$. Points without error bars represent the measured DT and DD yields uncorrected for neutron scattering, framed data points represent estimated birth-yield ratios determined from the measured data using a DSR -dependent correction (plotted vs measured apparent $DT T_{\text{ion}}$; same color-coding as in Figure 1). Error bars are statistical only; the systematic error is represented by the dotted curves compared to the dashed curve average for the framed data points. The solid black curve represents the expected birth yield ratio (plotted vs T_{thermal}) calculated using Bosch-Hale reactivities [38] assuming 50%:50% D:T; the dot-dashed black curve the same for 60%:40% D:T.

Non-hydrodynamic effects such as fuel stratification [35,49,50] and Knudsen tail depletion [36] have been proposed as possible mechanisms that could give rise to $DT T_{\text{ion}} > DD T_{\text{ion}}$. The fuel stratification hypothesis also implies that the DT yields would be larger relative to DD yields than expected from 1D hydrodynamic simulations [35]. The NIF $Y_{\text{DT}}/Y_{\text{DD}}$ result is in apparent contradiction with this hypothesis. In the Knudsen tail depletion hypothesis, ions from the high-energy tail of the distribution with mean free path much longer than the system scale size are lost from the reacting region before undergoing fusion. This narrows the width of the neutron energy distribution, reducing inferred apparent T_{ion} . At a Knudsen number of 0.05 and thermal T_{ion} of 5 keV, the expected T_{ion} ratio due to this effect alone would be 0.95 [37]. However, nominal Knudsen numbers calculated for the neutron-producing compression phase of these implosions are too small for the depletion to be significant at $(1-3) \times 10^{-3}$. Local Knudsen numbers might increase due to turbulence and mix, elevating the impact of this effect [37], but

such small-scale turbulence is expected to be reduced by viscosity [51].

3D dynamics seeded by laser drive asymmetry, engineering features, ice-layer non-uniformity etc. are believed to play a substantial role in these implosions [52-55]. Profile/reactivity effects, differential scatter and non-thermal flows in a realistic 3D implosion model have the potential to explain the DD/DT T_{ion} ratio measurements without invoking non-hydrodynamic effects. Asymmetry-driven 3D effects can be expected to introduce significant fuel flows. Presuming the bulk fluid flow is either strictly radial [24] or uniformly turbulent [23], broadening of the neutron spectrum is the same independent of viewing direction. However, given the nature of the assumed asymmetry seeds, highly resolved 3D simulations show strong velocity variance in the implosions, and line-of-sight (LOS) variations in apparent T_{ion} . Figure 3 shows the observed variations in DT (DD) apparent T_{ion} between the individual measurements in five (three) different LOS. The measurements conclusively rule out LOS anisotropy above 0.4 keV, and no anisotropy trend is seen with increasing apparent T_{ion} . Given the almost direct correlation between increasing apparent T_{ion} and increasing implosion velocity, the lack of a trend indicates that low-mode asymmetries are not amplified when implosion velocity increases.

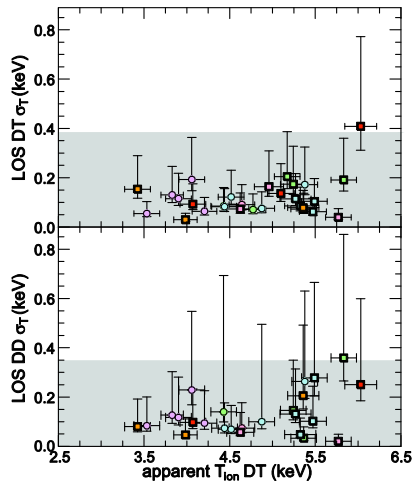


Figure 3: T_{ion} isotropy data as a function of apparent DT T_{ion} . The color-coding is the same as in Figure 1. (a) Observed variation in the DT apparent T_{ion} between the five available viewing directions, calculated as the r.m.s. between the individual data points and the average of all values for each shot. The vertical error bars represent the 68% confidence interval calculated by taking the square root of the ratio of the variance of the LOS T_{ion} measurements to the reduced χ^2 for the number of degrees of freedom corresponding to the upper and lower probabilities defining the confidence interval; the gray region represents an estimate of the systematic uncertainty. (b) Same as (a) for the three available viewing directions for apparent DD T_{ion} .

For DT, the highest observed anisotropy is seen for shot N150318 (right-most point in Figure 3), which was purposely imploded with a top-down $\pm 4\%$ laser drive asymmetry to provoke flows in the implosion. The limited LOS coverage may

lead to under-sampling of the signatures of velocity variance, which is being addressed through the addition of another detector system at the NIF. Improvements in capsule coverage and in the systematic measurement uncertainties are required to explore the T_{ion} variance in finer detail and to further investigate the 3D dynamics hypothesis. We conjecture that the small line-of-sight variations observed may indicate that flows due to low-mode asymmetries are not responsible for the observed DD/DT T_{ion} ratios; flows due to high-mode asymmetries, on the other hand, could simultaneously explain the data in Figure 1 and Figure 3.

Although the implosion dynamics for Indirect Drive Exploding Pushers (IDEPs) [56] are very different from cryogenically layered implosion dynamics, it is interesting to compare the measurements and simulations for these types of implosions. For the IDEPs, excellent agreement has been found between measured data and HYDRA simulations, with measured DT and DD yields and T_{ions} all showing agreement with simulated results. T_{ion} ratios of 0.84-0.90 observed for the IDEPs appear to be fully explained by profile effects alone; yield ratios also agree with expectation. Detailed analysis of DT neutron spectra from IDEPs have also shown that an observed non-Gaussian peak shape, due to profile effects, was correctly captured in simulations [57].

Given that neutrons from many different fuel elements at different temperatures and in different states of motion contribute to the measured spectra, a detailed comparison of measured and simulated spectral shape is another potential path to conclusive answers. Further refinements in analysis [58] and measurement techniques are under development, which may allow more sophisticated analysis of higher moments (skew, kurtosis) of the neutron peak in future work.

In summary, measured apparent DT T_{ions} from cryogenically layered NIF DT implosions are seen to be consistently higher than apparent DD T_{ions} , a discrepancy that increases with increasing T_{ion} . DD yields are observed to be high relative to DT yields, and LOS variations in T_{ion} measurements are small. Apparent DT and DD T_{ions} do not match 1D hydrodynamic simulations assuming a central, isobaric hot-spot. Species separation and non-Maxwellian ion distributions have been proposed as explanations for DT $T_{\text{ion}} > DD T_{\text{ion}}$; while a contribution from these effects cannot be ruled out, neither effect on its own self-consistently explains the present data. 3D profile/reactivity effects, differential scatter and bulk fluid motion have the potential to explain the measurements. Testing this 3D hypothesis requires highly resolved simulations. The present data provide a strong constraint for the 3D simulations in that they must simultaneously recreate large DT to DD T_{ion} differences (Figure 1) and small LOS variations (Figure 3). A complete understanding of implosion dynamics and hot-spot formation will be obtained by bringing to bear all available diagnostic measurements, and comparing the results obtained to realistic 3D simulations of the implosions.

The authors sincerely thank the NIF operations staff who supported this work. This work was performed under the auspices of the U.S. Department of Energy by Lawrence Livermore National Laboratory under Contract DE-AC52-07NA27344.

References

1. B.M. Van Wontergem et al., Fusion Science and Technology **69**, 452-469 (2016).
2. O.A. Hurricane et al., Nature **506**, 343-348 (2014); O.A. Hurricane et al., Phys. Plasmas **21**, 056314 (2014)
3. H.S. Park et al., Phys. Rev. Lett., **112**, 055001 (2014)
4. C. Cerjan, P.T. Springer, and S.M. Sepke, Phys. Plasmas **20**, 056319 (2013).
5. A.L. Kritcher et al., Phys. Plasmas **21**, 042708 (2014)
6. J.D. Kilkenny et al., Fusion Science and Technology **69**, 420-451 (2016)
7. V. Glebov et al., Rev. Sci. Instrum. **81**, 10D325 (2010)
8. M. Gatu Johnson et al., Rev. Sci. Instrum. **83**, 10D308 (2012).
9. V. Yu. Glebov et al., Rev. Sci. Instrum. **83**, 10D309 (2012)
10. R. Hatarik et al., J. Appl. Phys. **118**, 184502 (2015)
11. T.J. Clancy et al., SPIE Proceedings Vol. 9211, 92110A (2014).
12. G.P. Grim, G.L. Morgan, R. Aragonéz, T.N. Archuleta, D.E. Bower, C.R. Danly, O.B. Drury, J.M. Dzenitis, V.E. Fatherley, B. Felker, D.N. Fittinghof, N. Guler, F.E. Merrill, J.A. Oertel, C.H. Wilde, and M.D. Wilke, Proc. SPIE **8854**, 88540G (2013)
13. J.A. Frenje *et al.*, Rev. Sci. Inst. **72**, 854 (2001)
14. J.A. Frenje *et al.*, Phys. of Plasmas **17**, 056311 (2010).
15. D.T. Casey *et al.*, Rev. Sci. Instrum. **84**, 043506 (2013)
16. D.L. Bleuel et al., Rev. Sci. Instrum. **83**, 10D313 (2012).
17. G. Lehner and F. Pohl, Zeitschrift für Physik **207**, 83 (1967)
18. M.M.R. Williams, J. Nucl. Energy **25**, 489 (1971)
19. H. Brysk, Plasma Phys. **15**, 611 (1973).
20. L. Ballabio, J. Källne and G. Gorini, Nuclear Fusion **38**, 1723 (1998).
21. M.D. Cable and S.P. Hatchett, J. Appl. Phys. **62**, 2233 (1987).
22. T. J. Murphy, R. A. Lerche, C. Bennett, and G. Howe, Rev. Sci. Instrum. **66**, 930 (1995).
23. T. J. Murphy, Phys. Plasmas **21**, 072701 (2014).
24. B. Appelbe and J. Chittenden, Plasma Phys. Control. Fusion **53**, 045002 (2011).
25. V. Yu. Glebov et al., Bull. Am. Phys. Soc. **53**, PO8 5 (2011)
26. J.D. Kilkenny et al., Journal of Physics: Conference Series **688**, 012048 (2016)
27. The detectors have fast-response Bibenzyl scintillators as the detecting medium, each coupled to 3 photo-multiplier tubes and one photo-diode to allow for optimal detection over a large range of yields.
28. D.T. Casey et al., Phys. Rev. Lett. **115**, 105001 (2015)
29. T. Ma et al., Phys. Rev. Lett. **114**, 145004 (2015)
30. L. Berzak-Hopkins et al., Phys. Rev. Lett. **114**, 175001 (2015)
31. T. Doeppner et al., Phys. Rev. Lett. **115**, 055001 (2015).
32. See supplemental material at [] for shot-by-shot information.
33. Down-scatter ratio is defined as yield in the $E_n=10-12$ MeV range divided by yield in the $E_n=13-15$ MeV range; $\rho R \sim 20.4 \times DSR$ g/cm² (derived from an ensemble of CH simulations; similar work is underway for HDC which is expected to be close to the same).
34. J. A. Frenje et al., Nucl. Fusion **53**, 043014 (2013)
35. A. Inglebert, B. Canaud, and O. Larroche, EPL **107**, 65003 (2014).
36. K. Molvig, N.M. Hoffman, B.J. Albright, E.M. Nelson, and R.B. Webster, Phys. Rev. Lett. **109**, 095001 (2012).
37. G. Kagan, D. Svyatskiy, H.G. Rinderknecht, M.J. Rosenberg, A.B. Zylstra, and C.-K. Huang, Phys. Rev. Lett. **115**, 105002 (2015); G. Kagan, private communication.
38. H.-S. Bosch and G.M. Hale, Nucl. Fusion **32**, 611 (1992)
39. M.M. Marinak, G.D. Kerbel, N.A. Gentile, O. Jones, D. Munro, S. Pollaine, T.R. Dittrich, and S.W. Haan, Phys. Plasmas **8**, 2275 (2001).
40. A.L. Kritcher et al., Phys. Plasmas **23**, 052709 (2016).
41. D.B. Sayre, L.A. Bernstein, J.A. Church, H.W. Herrmann, and W. Stoeffl, Rev. Sci. Instrum. **83**, 10D905 (2012).
42. F.E. Merrill et al., Rev. Sci. Instrum. **83**, 10D317 (2012).
43. D.G. Hicks, B.K. Spears, D.G. Braun, R.E. Olson, C.M. Sore, P.M. Celliers, G.W. Collins, and O.L. Landen, Phys. Plasmas **17**, 102703 (2010); D.G. Hicks et al., Phys. Plasmas **19**, 122702 (2012).
44. M. Gatu Johnson et al., Phys. Plasmas **20**, 042707 (2013).
45. $Y \sim \rho^2 \times \langle \sigma v(T_{ion}) \rangle \times V \times \tau_{burn} \sim (P/T)^2 \times \langle \sigma v(T_{ion}) \rangle \times V \times \tau_{burn}$; for DT from 2-7 keV, $\langle \sigma v(T_{ion}) \rangle \sim T_{ion}^{-4}$. With constant V and τ_{burn} , $Y \sim (PT_{ion})^2$.
46. MCNPX Version 2.5.0 User's Manual (LA-CP-05-0369, April 2005) <https://mcnpx.lanl.gov/>
47. The MCNPX model is made up of a spherical core (radius 35 μ m and DT gas density $\rho=122.5$ g/cm³), surrounded by a DT shell (35-50 μ m) with density varied to obtain different values for dsr , and a CH shell (50-55 μ m, $\rho=250$ mg/cm³). A thermal neutron source with $T_{ion}=4$ keV, Gaussian distributed in space from 0-35 μ m is used in separate DD and DT runs, and escaped neutron spectra are tallied using point detectors. The resulting correction factor is $(Y_{DDmeas}/Y_{DDbirth}) / (Y_{DTmeas}/Y_{DTbirth}) = 24.27 \times dsr^2 - 6.93 \times dsr + 1$.
48. C.K. Li et al., Phys. Plasmas **7**, 2578 (2000)
49. D.T. Casey et al., Phys. Rev. Lett. **108**, 075002 (2012).
50. H.G. Rinderknecht et al., Phys. Rev. Lett. **114**, 025001 (2015).
51. C.R. Weber, D.S. Clark, A.W. Cook, L.E. Busby, and H.F. Robey, Phys. Rev. E **89**, 053106 (2014)
52. J.R. Rygg et al., Phys. Rev. Lett. **112**, 195001 (2014).
53. C.R. Weber et al., Phys. Plasmas **22**, 032702 (2015).
54. B.K. Spears et al., Phys. Plasmas **22**, 056317 (2015).
55. D. Clark et al., Phys. Plasmas **22**, 022703 (2015).
56. S. LePape et al., Phys. Rev. Lett. **112**, 225002 (2014).
57. Laurent Divol, private communication (2015).
58. D.H. Munro, Nucl. Fusion **56**, 036001 (2016).